

# Controlled cavitation in microfluidics

Ed Zwaan,<sup>1</sup> Séverine Le Gac,<sup>2</sup> Kinko Tsuji,<sup>3</sup> and Claus-Dieter Ohl<sup>1</sup>

<sup>1</sup>Faculty of Science and Technology, Physics of Fluids,  
University of Twente, Postbus 217, 7500 AE Enschede, The Netherlands.

<sup>2</sup>BIOS the Lab-on-a-Chip group, MESA+ Institute for Nanotechnology,  
University of Twente, Postbus 217, 7500 AE Enschede, The Netherlands.

<sup>3</sup>Shimadzu Europa GmbH, Albert-Hahn-Strasse 6-10, D-47269 Duisburg, Germany.

(Dated: February 20, 2007)

We report on cavitation in confined microscopic environments which are commonly called microfluidic or lab-on-a-chip systems. The cavitation bubble is created by focusing a pulsed laser into these structures filled with a light-absorbing liquid. At the center of a  $20\ \mu\text{m}$  thick and 1 mm wide channel pancake-shaped bubbles expand and collapse radially. The bubble dynamics compares with a two-dimensional Rayleigh model and a planar flow field during the bubble collapse is measured. When the bubble is created close to a wall a liquid jet is focused towards the wall, resembling the jetting phenomenon in axisymmetry. The jet flow creates two counter-rotating vortices which stir the liquid at high velocities. For more complex geometries, e.g. triangle- and square-shaped structures, the number of liquid jets recorded correlates with the number of boundaries close to the bubble.

*Introduction* Approximately 100 years ago it had been revealed that cavitation bubbles are a threat to almost any material in contact with high speed flows; cavitation causes wear on pump blades, at bends in flow lines, and cavitation can disintegrate ship propellers [1–3]. One reason why cavitation is so aggressive lies in its ability to focus fluid flows to very small scales; the bubbles concentrate the energy from the fluid during their shrinkage. The violence of the bubble collapse is evident from the emission of shock waves and light [4], and their catalytic effect on chemical reactions [5]. Only recently the attention from largely free cavitation bubbles [6] has shifted towards confined bubbles [7]. Still, rather few modeling efforts are reported on confined bubble dynamics under the consideration of *high Reynolds numbers*, e.g. [8]. This Letter reports on an experimental study of cavitation dynamics occurring in a narrow gap and close to additional boundaries with unprecedented detail. The confining geometry is adapted from microfluidic systems [9] or so called lab-on-a-chip devices. In these geometries low Reynolds number flows are typically found. However, due the rapidness of cavitation bubble-induced flows challenging actuation in microfluidics can be met. Here we will demonstrate that cavitation bubbles are able to actuate flows on a microsecond time scale. After an introduction of the experimental setup we will first discuss in this Letter the dynamics of a bubble in a planar geometry and then present the liquid focusing and jetting of bubbles close to one, two, and more boundaries.

*Experimental setup* These experiments are stimulated by the work of Chen *et al.* [10]. The group studied the interaction of a stable gas bubble with a laser-induced cavitation bubble in a  $10\ \mu\text{m}$  thick gap of fluid. Additionally to the stroboscopic recording used in their work we adopt a framing camera operating at 1 million frames/s (HPV-1, Shimadzu Corp., Kyoto, Japan). Also, the fluid gap is replaced by microfluidic structures, see below. The bubble is generated with an expanded beam from a pulsed and frequency-doubled Nd:YAG laser (Solo PIV, New Wave, Fremont, CA, USA). The energy

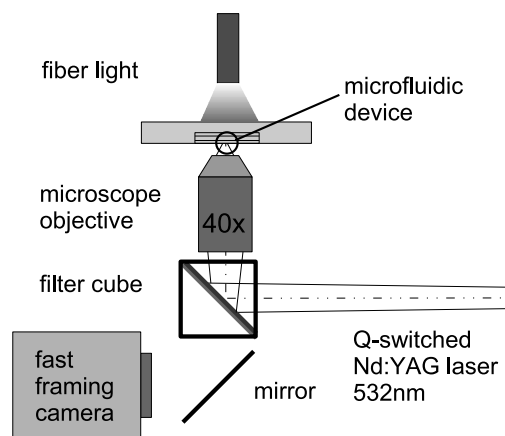


FIG. 1: Sketch of the experimental setup to generate cavitation bubbles in microfluidic devices. A slightly divergent beam from a pulsed laser is focused into the fluid filled structures positioned in the image plane of the inverted microscope. The bubble dynamics is imaged with a high speed framing camera at 1 million frames/s.

of the laser pulses is in the range  $5 - 50\ \mu\text{J}$  and have a duration of 6 ns. The sketch, Fig. 1, shows that the laser beam is not collimated but slightly divergent; thus, after proper alignment the focus of the laser beam and the image plane of the 40x objective of the inverted microscope (CF 40, Carl Zeiss GmbH, Göttingen, Germany) superimpose allowing in-focus images of the bubble outline. A filter block reflects only the green laser light and lets pass all other wavelengths for proper illumination with a fiber lamp (ILP-1, Olympus, Zoeterwoude, The Netherlands). The reproducibility of the experiments enables to take stroboscopic pictures to record especially the bubble expansion at higher temporal resolution. Therefore, a single-frame camera (PCO Imager Intense, Kehlheim, Germany) is combined with a short flash light (11 ns flash duration, Nanolite KL-M, HSPS, Germany) and a variable delay generator.

Lab-on-a chip devices are fabricated in an elastomeric

material, PDMS (polydimethylsiloxane) using conventional molding procedure. A silicon mold is first fabricated in a clean-room environment using photolithography and dry-etching techniques (Bosch process). A mixture of a PDMS pre-polymer and a curing agent (10:1) (Sylgard 184, Dow Corning) is subsequently poured on the resulting mold and cured for 2 hours at 60°C. After curing, the PDMS slab is removed from the mold and reservoirs are punched using a needle. Finally, chips are bonded to a microscope glass slide or a polypropylene foil after plasma activation of the surface. Chips are filled with an aqueous solution of red dye (Direct Red 81, Sigma Aldrich, St. Louis, MO, USA). For flow visualization and quantitative analysis the liquid was seeded with small particles (2  $\mu\text{m}$  diameter, Duke Scientific, Fremont, CA, USA).

*Bubble dynamics in radial symmetry* The bubble dynamics in a 20  $\mu\text{m}$  high and 1 mm wide channel is due to the large distance between the bubble and the closest channel wall undisturbed; the flow field remains radial during the collapse. We observe no after-bounces following the first bubble collapse and the flow stops subsequently nearly instantaneously (within 2  $\mu\text{s}$ ). Interestingly, the expansion of the bubble proceeds faster than its shrinkage, see Fig. 2 a) [10]. Presumably, the vapor pressure from the initial hot bubble drives the bubble expansion, but cools down as the bubble expands leading to the asymmetry in the radius-time curve. Analyzing the particle motion reveals the propagation of a radial wave from the bubble center during the expansion stage; the wave is very likely propagating in the elastic PDMS. From now on we discuss the collapse phase of the bubble: accounting for the fluid inertia only the bubble dynamics can be compared with the pressure driven closure of a cylindrical void. A first justification for this approach is the high Reynolds number  $Re = 2R_{max}^2/\nu/t_c$  of  $Re = 530$  for a bubble collapsing from  $R_{max} = 43 \mu\text{m}$  within  $t_c = 7 \mu\text{s}$ ; with  $\nu = 10^{-6} \text{m}^2/\text{s}$  being the kinematic viscosity.

Originally Lord Rayleigh has derived an equation for the closure for a spherical void [3]; the here appropriate formulation for a planar, e.g. a 2-dimensional closure is discussed in Refs. [11]. This now cylindrical Rayleigh equation reads:

$$\left(R\ddot{R} + \dot{R}^2\right) \log \frac{R}{R_\infty} + \frac{1}{2}\dot{R}^2 = \frac{p}{\rho}, \quad (1)$$

where  $\rho$  is the liquid density,  $R_\infty$  is the distance at which the velocity in the fluid has dropped to zero, and  $p$  is the pressure far from the bubble which we assume constant,  $p = 10^5 \text{Pa}$ . The parameter  $R_\infty$  comes from the fact that the velocity decreases only with  $1/r$  in the liquid, thus for a finite energy of the fluid a cut-off has to be introduced. In the current experiments this can be easily accomplished because the distance  $R_\infty$  is identified with the geometrical constraints: the bubble is generated in the center of a 1 mm wide channel thus  $R_\infty$  is fixed to  $R_\infty = 0.5 \text{mm}$ . The comparison of the measured (circles) and calculated (solid line) bubble dynamics in Fig. 2 a) shows good agreement; in contrast the dashed line depicts

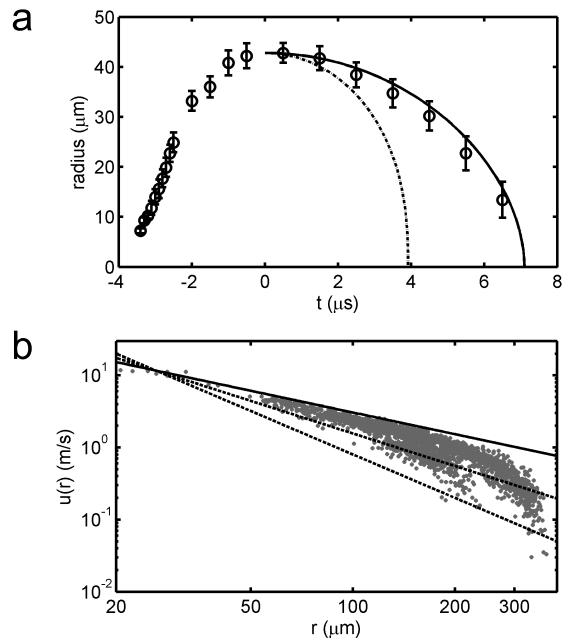


FIG. 2: (a) Comparison of the stroboscopically measured bubble radii ( $\circ$ ) and the model predictions for the 2D Rayleigh collapse (solid line) and 3D type (dashed line). The time  $t = 0$  is shifted to maximum bubble expansion  $R_{max} = 43 \mu\text{m}$ . (b) The velocity is plotted in a log-log graph as a function of the distance  $r$  from the bubble center. The solid line shows the predicted  $1/r$  scaling for a 2 dimensional flow, the two lower dashed lines depict a  $r^{-1.5}$  and a  $r^{-2}$  dependency, respectively.

the collapse dynamics for a 3-dimensional bubble predicting a much faster shrinkage than observed.

It might be argued, that due to the small channel height the boundary layer affects the bubble dynamics and viscosity has to be taken into account. A rough estimate of the distance,  $\delta$ , vorticity can grow from the wall into the channel is given by  $\delta = \sqrt{\nu t}$ . Thus, with a bubble lifetime of  $t = 11 \mu\text{s}$  we estimate  $\delta \approx 3 \mu\text{m}$  being smaller than half the channel height of 10  $\mu\text{m}$ .

To detail further if the bubble dynamics is indeed – as suggested by the good agreement with the 2D Rayleigh Eq. (1) – dominated by an inertial planar flow, the velocity as a function from the bubble center is analyzed.

In 2D the velocity of the liquid  $u(r, t)$  should follow the assumed  $1/r$  dependency. To check this dependency, we make use of the seed-particles in the flow as tracers for the local flow velocity by using a standard particle image velocimetry technique (PIV) [12] to cross-correlate interrogation areas from two successive frames. With this technique the locally averaged flow velocity is measured. It is important to note, that due to the large focal depth of the imaging optics not only particles in the center of the channel but also close to the bottom and top, thus within the boundary layer are imaged. Therefore, the flow velocity obtained from the PIV algorithm is a lower bound of the flow which we expect to be highest in the center of the channel. Figure 2 b) depicts the measured veloc-

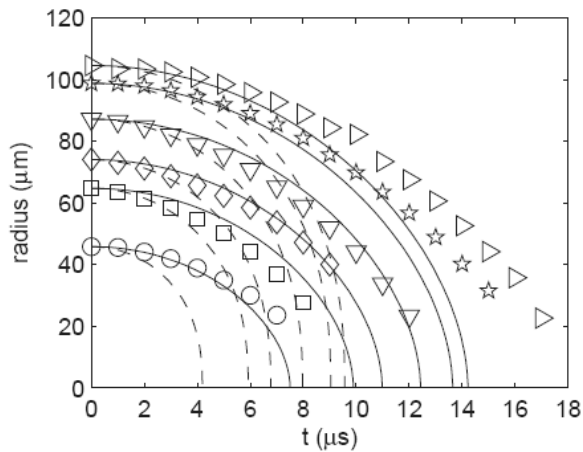


FIG. 3: Comparison of the bubble dynamics for different sized bubbles with a two dimensional model (solid line) and the 3D-Rayleigh collapse (dashed line). Markers are from measurements with the high-speed camera

ity (gray points) in the channel just one frame prior to bubble collapse; the bubble surface is located at  $r = 20 \mu\text{m} \pm 3 \mu\text{m}$ . The solid line denotes a curve with a  $1/r$  dependency, with  $u(r) = 3.06 \cdot 10^{-4} / r \text{ m}^2/\text{s}$  being a fit to the leftmost data points. This curve follows very nicely the *fastest* measured particles in the flow up to a distance of  $r = 180 \mu\text{m}$ . The two dashed curves depict a velocity dependency as  $r^{-1.5}$  and  $r^{-2}$ , respectively. Although the line for  $r^{-1.5}$  converges faster ( $u \rightarrow 0$ ) as  $r \rightarrow \infty$  it underestimates the velocities closer to the bubble wall. The message from the analysis summarized in Fig. 2 b) is that the velocity field in the center of the channel is best represented with a planar flow field.

However, it is expected that for larger bubbles the dynamics can not anymore be described with a simple inertia driven model, Eq. (1). Possibly because viscosity has more time to diffuse from the channel walls and effects the inflow. Additionally, for larger bubbles the laser energy is increased with the chance to create more non-condensable gas which might hinder the shrinkage, too. This lengthening of the shrinkage is documented in Fig. 3 revealing that the good agreement between the 2D bubble model (solid line) gets lost for larger bubbles, here when  $R_{max} > 90 \mu\text{m}$ .

*Close to a boundary* It is well known that a bubble collapsing at some stand-off distance from an infinite boundary [13, 14] develops an *inertia driven* flow focusing phenomena [15]. The proximity of the boundary disturbs the radial flow, e.g. it causes a faster inflow from the wall-distant part of the bubble interface. There flow becomes focused and a jet flow directed towards the rigid boundary [16] is generated. This jet flow travels through the bubble center, penetrates the lower bubble interface, and impacts onto the boundary where it creates a long lasting vortex ring [17]. We now want to test if comparable dynamics is found in a planar geometry. Figure 4 a) depicts the stages of a bubble expanding and shrinking at the channel boundary, see bright lower border. During shrink-

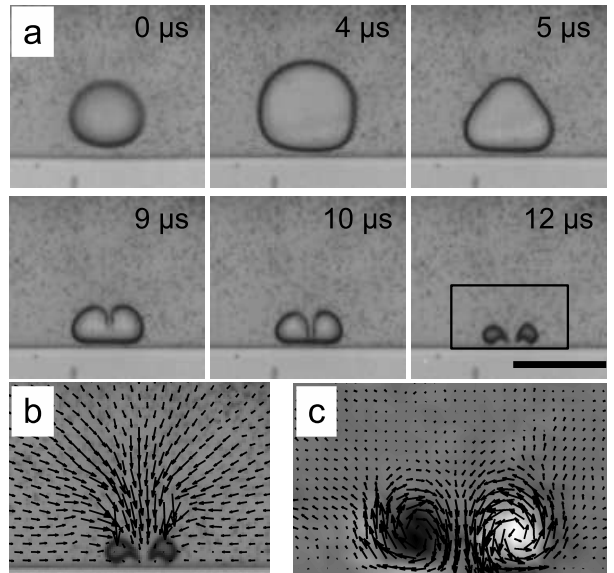


FIG. 4: Planar bubble dynamics close to a channel wall. (a) Selected frames from a high-speed recording depicting the formation of a liquid jet towards the wall. The bar indicates a length of  $150 \mu\text{m}$ . (b) Velocity field of the flow after the bubble has split up due to the impacting jet flow. The jet flow and the radial inflow impact and lead to a splashing phenomena (see text). The longest velocity vector corresponds to  $7.4 \text{ m/s}$ . (c) Vorticity plot after the bubble has collapsed averaged over the time interval  $t \in [24 \mu\text{s}; 64 \mu\text{s}]$ . Note, the bubble has already vanished during this time interval. Bright colors denote counter-clockwise rotation and dark ones clockwise.

age the bubble obtains a triangular shape. The top part of the bubble interface flips towards the boundary between  $t = 5 \mu\text{s}$  and  $t = 9 \mu\text{s}$  and thereby creates a jet with a tip diameter of approx.  $8 \mu\text{m}$ . It impacts with a velocity of roughly  $25 \text{ m/s}$  onto the boundary. Having a closer look, we find very similar features which have been reported in axisymmetric collapse in planar geometry, too. One of these is the splashing phenomena [18]: liquid is accelerated away from the wall –in a sort of splash– when the radial flow from the still shrinking bubble impacts onto the outwards spreading jet flow (noticeable by the kinks of the split bubbles in frame  $12 \mu\text{s}$  of Fig. 4 b). At later times the two tiny remains of the bubbles become entrained in two counter-rotating vortex rings. The vortex rings are revealed with PIV. An averaged flow field over  $40 \mu\text{s}$  after the jet impact is depicted in Fig. 4c. Tracing the maximum of the vorticity  $c = \nabla \times \underline{u}(x, y)$  within this time interval we find a decrease (not shown) from  $10^5 \text{ s}^{-1}$  to  $3 \cdot 10^4 \text{ s}^{-1}$ . Thus, the center of the vortex rotates with an initial rotation rate of more the 10.000 rotations/s!

*Jetting in more complex geometries* Confined bubbles in tubes have received attention in the medical field, for example cavitation in arteries produced in laser assisted angioplasty e.g. [19], and in diagnostic and therapeutic ultrasound applications [20]. In channels with rectangular-shaped cross sections we find that largely expanding bubbles become ellipsoidal, see Fig. 5 left. The lower row shows the resulting bubble shape

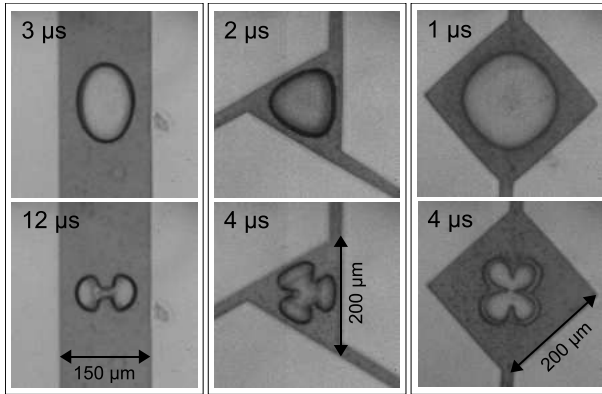


FIG. 5: Snapshots for three different geometries from left to right: single bubble cavitation in a  $150\ \mu\text{m}$  wide and several millimeter long channel, in a  $200\ \mu\text{m}$  isosceles triangular structure with feeding channel attached to the corners, and in a square chamber with  $200\ \mu\text{m}$  long sides. From the time stamps it becomes evident, that the jetting flow is much faster in the latter two cases.

after jets have developed. Here, as in the next two discussed cases jets develop always during the shrinkage and at locations of the interface where most fluid is available. For the  $150\ \mu\text{m}$  wide channel, two jets develop in opposite directions flowing along the channel. At a later stage (not shown in Fig. 5) these jets impact and reflect towards the channel walls causing the transport of vorticity to the walls. In the second and third example of Fig. 5 again jetting is found from interface areas where liquid is most easily "accessible": a bubble oscillating inside a triangular structure develops fast jets starting from the feeding capillaries placed at the corners, Fig. 5 center. A similar observation is found in a square geometry (Fig. 5 right); here four jets start from the corners, two of them being connected to feeding capillaries. This geometry leads to a bubble shape resembling a four-leaved clover. At later stage we find for the triangular and the square chambers reflections of the inflowing jets and complex bubble breakup indicating that the planar flow field becomes lost.

*Discussion and conclusions* In general the essentially planar bubble dynamics presented in this Letter resembles the one observed in spherical and axisymmetry. Far from boundaries the collapse of the bubble can be described with a radial velocity potential leading to a  $1/r$  drop of the velocity as compare to the  $1/r^2$  dependency in spherical symmetry. Yet, larger bubbles (in our case above  $R_{max} > 90\ \mu\text{m}$ ) collapse slower, and this is likely due to viscous effects. Although we have emphasized that the bubbles exhibit an essentially planar flow – as the collapse progresses – the bubble will shrink to a size smaller than the channel height. Then a 3-dimensional flow will set in. Cavitation in microfluidics allows for reaching a regime of high Re-numbers for microsecond time scales. The important finding that jetting and creation of vorticity occur has immediate practical applications. Jetting flows can be utilized for microfluidic pumping [21], and vorticity creation for vigorous mixing on short time scales. A visualization of

the flow field is much easier to achieve in a planar geometry than in axisymmetry [22] which is demonstrated in the nicely resolved vortex structures generated after the jet impact, Fig. 4. Cavitation is a tool which allows for scaling down fluid handling to a microfluidic environment preserving the benefits of high Re-number flows. The added benefit of laser created bubbles is the non-invasive generation mechanism. No connecting wires or actuators are necessary and the position of actuation can suitably be addressed by scanning the laser spot with mirrors.

The authors are grateful for the discussions with Prof. Andrea Prosperetti, Prof. Detlef Lohse, and Dr. Evert Klaseboer. We thank Jiajie Li for Si-mold fabrication. C.D.O. is supported by N.W.O. (The Netherlands) through a VIDI grant.

- 
- [1] D. Silberrad, *Engineering* Jan. 12, 33 (1912).
  - [2] M.S. Plesset and A. Prosperetti, *Annu. Rev. Fluid Mech.* **9**, 145 (1977).
  - [3] T.G. Leighton, *The Acoustic Bubble* (Academic Press, London, 1994). C.E. Brennen, *Cavitation and bubble dynamics*. (Oxford University Press, New York, 1995).
  - [4] M.P. Brenner, S. Hilgenfeldt, and D. Lohse, *Rev. Mod. Phys.* **74**, 425 (2002).
  - [5] K.S. Suslick, Y. Didenko, M.M. Fang, T. Hyeon, K.J. Kolbeck, W.B. III McNamara, M.M. Mdeleleni, M. Wong, *Phil. Trans. Roy. Soc. A* **357** 335 (1999).
  - [6] D. Lohse, *Physics Today* **56** 36 (2003).
  - [7] V.S. Ajaev, G.M. Homsy, *Annu. Rev. Fluid Mech.* **38** 277 (2006).
  - [8] H. Yuan, H.N. Oğuz, and A. Prosperetti, *Int. J. Heat Mass Transf.* **42** 3643 (1999).
  - [9] T.M. Squires and S.R. Quake, *Rev. Mod. Phys.* **77** 977 (2005).
  - [10] Y.H. Chen, H.Y. Chu, and L. I, *Phys. Rev. Lett.* **96** 034505 (2006).
  - [11] H.N. Oğuz and A. Prosperetti, *J. Fluid Mech.* **257** 111 (1993). D. Lohse, R. Bergmann, R. Mikkelsen, C. Zeilstra, D. van der Meer, M. Versluis, K. van der Weele, M. van der Hoef, and H. Kuipers, *Phys. Rev. Lett.* **93** 198003 (2004).
  - [12] We use the package urapiv from <http://urapiv.wordpress.com/>. Two consecutive images are evaluated on  $16 \times 16$  pixels interrogation windows with 4 pixels overlap.
  - [13] M.S. Plesset and R.B. Chapman, *J. Fluid Mech.* **47** 283 (1971).
  - [14] W. Lauterborn and H. Bolle, *J. Fluid Mech.* **72** 391 (1975).
  - [15] M.P. Brenner, *Nature*, **403** 377 (2000).
  - [16] A. Philipp and W. Lauterborn, *J. Fluid Mech.* **361** 75 (1998).
  - [17] T.B. Benjamin and A.T. Ellis, *Phil. Trans. Roy. Soc. Lond. Ser. A* **260** 221 (1966).
  - [18] E.A. Brujan, G.S. Keen, A. Vogel, and J.R. Blake, *Phys. Fluids*. **14** 85 (2002).
  - [19] A. Vogel, R. Engelhardt, U. Behnle, and U. Parlitz, *Appl. Phys. B* **62** 173 (1996).
  - [20] P. Zhong, Y. Zhou, and S. Zhu, *Ultrasound Med. Biol.* **27**, 119 (2001). T. Ye, J.L. Bull, *J. Biomech. Eng.* **128** 554 (2006). E. Sassaroli, K. Hynynen, *Appl. Phys. Lett.* **89** 123901 (2006).
  - [21] B.C. Khoo, E. Klaseboer, and K.C. Hung, *Sens. Actuators A* **118** 152 (2005). K.S.F. Lew, E. Klaseboer, and B.C. Khoo, *Sens. Actuators A* **133** 161 (2007).
  - [22] A. Vogel, W. Lauterborn, R. Timm, *J. Fluid Mech.* **206** 299.